Hydrophobic Free Energy Eigenfunctions of Pore, Channel, and Transporter Proteins Contain β-Burst Patterns

Karen A. Selz,*#§ Arnold J. Mandell,*#§ and Michael F. Shlesinger¶

*Cielo Institute, Asheville, North Carolina 28804; #Department of Psychiatry and Behavioral Sciences, Emory University School of Medicine, Atlanta, Georgia 30322; §Department of Mathematical Sciences, Florida Atlantic University, Boca Raton, Florida 33431; and ¶Physical Sciences Division, Office of Naval Research, Arlington, Virginia 22217 USA

ABSTRACT Hydropathy plots are often used in place of missing physical data to model transmembrane proteins that are difficult to crystallize. The sequential maxima of their graphs approximate the number and locations of transmembrane segments, but potentially useful additional information about sequential hydrophobic variation is lost in this smoothing procedure. To explore a broader range of hydrophobic variations without loss of the transmembrane segment-relevant sequential maxima, we utilize a sequence of linear decompositions and transformations of the n-length hydrophobic free energy sequences, $H_{i,\,i=1\ldots n}$, of proteins. Constructions of hydrophobic free energy eigenfunctions, ψ_l, from M-lagged, $M \times M$ autocovariance matrices, C_M, were followed by their all-poles, maximum entropy power spectral, $S_\omega(\psi_l)$, and Mexican Hat wavelet, $W_{a,b}(\psi_l)$, transformations. These procedures yielded graphs indicative of inverse frequencies, ω^{-1}, and sequence locations of hydrophobic modes suggestive of secondary and supersecondary protein structures. The graphs of these computations discriminated between Greek Key, Jelly Role, and Up and Down categories of antiparallel β-barrel proteins. With these methods, examples of porins, connexins, hexose transporters, nuclear membrane proteins, and potassium but not sodium channels appear to belong to the Up and Down antiparallel β-barrel variety.

INTRODUCTION

In addition to discriminating α-helical from β-barrel transmembrane domains by using a series of linear transformations of their primary sequences, it may also be possible to discriminate among the common β-barrel configurations. These include the parallel β-strands arranged in closed barrels or open twisted sheets, in which β-strands are interspersed with helical segments as in α/β proteins and antiparallel β-strands. Depending upon their patterns of connectivity, the latter can be of Up and Down, Greek Key, or the Jelly Role Barrels type (Richardson, 1975, 1977; Wilmot and Thornton, 1988; Richardson and Richardson, 1990).

Individual amino acid hydrophobic free energies, hydrophobicities, $H_{i,\,i=1\ldots n}$ in kcal/mol, are computed from each amino acid's relative equilibrium concentrations in a binary, aqueous-organic solvent (Nozaki and Tanford, 1971) or a condensed vapor partition (Kyte and Doolittle, 1982). Characteristic patterns in the sequences of amino acid side-chain hydrophobicities are generally acknowledged to play a significant role in the determination of the secondary structure of proteins (Levitt and Chothia, 1976; Rose, 1978). In an aqueous environment, secondary turn formation, facilitated by in-line surface-minimizing attraction between statistically phase coherent hydrophobic patches, involves the cooperative interactions of the hundreds to thousands of hydrogen bonds of the surrounding water solvent (Eisenberg and Kauzmann, 1968). In high dielectric constant, extramembranous, aqueous solvent, the sequential patterns of relative hydrophobicity in amino acid chains are known to strongly influence whether, for example, segments of peptide chains of globular proteins roll up into α-helices with a hydrophobic mode of $\omega^{-1} \approx 3.6$ aa (amino acids) per turn (from low to high to low again in side-chain hydrophobic values), or, for most β-strands, $\omega^{-1} \approx 2.3$–2.6 aa per rotation (Eisenberg et al., 1984).

Analyses of the secondary structures in the low dielectric constant, lipophilic, intramembranous, transmembrane segments of physically well-characterized transmembrane proteins such as bacteriorhodopsin demonstrate hydrophobic sequences such that the helical wavelength is maintained but the relative amphophilic organization is rotated $\sim$180° in phase (Engelman et al., 1986; Henderson et al., 1990). In contrast with helical arrangements in extramembranous environments, external residues of transmembrane segments are more hydrophobic on the average than those facing the internal, more hydrophilic "channel," while maintaining characteristic α-helical rotation lengths of $\omega^{-1} \approx 3.6$ amino acids. This suggests that the same principles governing hydrophobic rotation may apply in both aqueous and transmembrane environments (Rees et al., 1989).

The technique commonly used for conjecture about the lengths and locations of transmembrane segments in membrane-associated proteins is called a hydropathy plot (Kyte and Doolittle, 1982). This is a graph of a windowed moving average (the choice of window size being arbitrary) across the hydrophobicity sequence of membrane proteins. The largest positive variations are interpreted as the lipophillic, hydrophobic transmembrane segments of the proteins (Fasman and Gilbert, 1990). The seminal finding is that of the

Received for publication 18 March 1998 and in final form 20 July 1998.

Address reprint requests to Dr. Karen A. Selz, Cielo Institute, 486 Sunset Drive, Asheville, NC 28804. Tel.: 704-251-9794; Fax: 704-254-4431; E-mail: cieloinst@aol.com.

0006-3495/98/11/2332/11 $2.00

seven sequential hydrophobic maxima, each ~25 aa apart, seen in the hydropathy plots of bacteriorhodopsin, thought to be the evolutionary prototype of the G-protein gene superfamily of seven transmembrane receptors (Engelman et al., 1986; Henderson et al., 1990). The long-standing premise that the transmembrane segments of this G-protein-coupled protein are composed of seven transmembrane α-helical segments has been confirmed by physical evidence, such as that from projection maps (Unger et al., 1997) and high-resolution electron cryomicroscopy (Kimura et al., 1997) of bacteriorhopsin. Because membrane proteins are particularly difficult to crystallize and, therefore, to study by direct physical methods, very few membrane-associated proteins have been studied with x-ray diffraction at high resolution. This makes computational techniques facilitating consistent conjectures about the structure of membrane proteins from amino acid sequence data valuable (Engelman et al., 1986; Fasman and Gilbert, 1990).

The generality of the α-helical composition of transmembrane segments, as inferred from length and location of maxima in hydropathy plots of membrane-associated proteins, has come increasingly into question. Besides the rhodopsins, among the few available x-ray crystallographic studies of transmembrane proteins are those involving porins, such as the 362 aa *Escherichia coli* OmPF, which manifests a hydropathy plot with 16 maxima. Physical studies of this protein revealed a trimeric arrangement of 16-stranded, membrane-spanning sets of antiparallel β-strands joined by top and bottom loop domains. These structures form the β-barrels characteristic of solvent-accessible pores (Pauptit et al., 1991b; Cowan et al., 1995). The hydrophobic transmembrane segments of most, if not all, of the porins are observed as 16 maxima in the hydropathy plot. This is even true of the 301-residue porin of *A. Rhodobacter capsulatus*, with little sequence similarity to that of *E. coli* (Pauptit et al., 1991b).

Thus when the family of five passive-mediated transmembrane hexose transporters, the GLUTs, were cloned and demonstrated about 12 hydropathy plot maxima (see Silverman, 1991; Elias and Longo, 1992 for the history), some groups interpreted these maxima as transmembrane α-helices, reflecting the choice of G-protein receptors as the relevant analogy (Mueckler et al., 1985). Others considered the greater number of smaller hydrophobic maxima and argued that the GLUTs were more like the 16 antiparallel β-strands composing the β-barrels of the porins. This latter approach led to an alternative folding model for the GLUTs (Fischbarg et al., 1994). Definitive x-ray crystallographic and nuclear magnetic resonance data are not yet available to resolve this debate about the passive sugar transport membrane proteins.

The arbitrary choice of the size of the averaging window used in construction of the hydropathy plot may be relevant to this debate. For example, the earlier studies of the GLUTs (Mueckler et al., 1985; Baldwin, 1990) used a 21-aa window to include "enough to form a transmembrane α-helix," and they found 12 transmembrane segments of 21 residues each. Another approach also led to a porin-like β-barrel hypothesis for the GLUT family of transporters (Fischbarg et al., 1994). The choice of an asymptotically smoothing, iterative nearest-neighbor averaging technique yields other results (compare the hydropathy plots of the putative 12 transmembrane segment containing epithelial porin with the $\geq$12 maxima of the fructose transporter, a member of the GLUT family, in Fig. 2). In analogy to some inferences made about the GLUTs, the transmembrane segments of the biogenic amine transporters are often called α-helices (Gu et al., 1994, 1996), although some investigations of these plasma membrane neurotransmitter transporters have revealed conductance behavior suggesting a functional similarity to the β-barrel porins (Sonders and Amara, 1996).

This study explores the possibility that n-length transmembrane proteins with distinctive domain topologies and patterns of connectivity can be discriminated by using a set of relatively standard computational techniques (Broomhead and King, 1986; Golub and Van Loan, 1993; Madan, 1993; Wickerhauser, 1994; Mandell et al., 1997a,b,c, 1998). These include the linear decomposition of lagged, $M = 16$ order autocovariance matrices, C_M, of their primary aa sequences as hydrophobic free energies $H_{i,\, i = 1 \ldots n}$. This is followed by hydrophobic free energy eigenfunction, ψ_l, construction, all-poles maximum entropy power spectra, $S_\omega(\psi_l)$, and Mexican Hat wavelet, $W_{a,b}(\psi_l)$, transformations. These procedures lead to a set of hydrophobic modes as inverse frequencies, ω^{-1} in aa, that are characteristic of the protein under study. $W_{a,b}(\psi_l)$ serves as an independent check on the ω^{-1} aa elucidated by $S_\omega(\psi_l)$, as well as localizing the mode densities in the aa sequence. These procedures have led to conjectures about secondary structures and sequences of secondary structures in membrane and globular proteins that are consonant with physical data and have produced discomfirmable, experimentally supported predictions of mode matches between peptide ligands and membrane receptors (Mandell et al., 1997a,b,c, 1998).

The morphologies of the graphs of the leading eigenfunctions, ψ_1, coincide closely with the hydropathy plots of seven transmembrane, G-protein-coupled receptors (Mandell et al., 1997a, 1998). To be consistent with this observation, in our computations we often choose the value of M, the number of lags in the data matrix and order of the $M \times M$ autocovariance matrices, to minimize least-squares deviation of ψ_1 from the hydropathy plot. Because $M = 16$ met this criterion for the majority of the proteins studied here, and for the sake of comparison, a constant $M = 16$ was selected. The $S_\omega(\psi_l)$ of the secondary eigenfunctions (i.e., $l = 2$ and/or 3) discriminate among transmembrane receptor proteins by the use of additional sequential structural information. The dominant ω^{-1}'s of $S_\omega(\psi_2)$ demonstrate matches with the peptide ligand-binding modes located in the extracellular domains (Mandell et al., 1997a, 1998). In this study, we take a similar approach to transmembrane proteins without the receptor sites characteristic of G-coupled proteins. Here we predict the secondary structure(s) of the transmembrane segments of pore, channel, and transporter proteins.

It is well known that the sequential structure of polypeptide and protein loops can be variable in length and hydrophobic mode structure. Homologous proteins demonstrate the greatest number of insertions and deletions in their loop structures, and intron positions are found at sites in structural genes that correspond to loop regions in the protein structure. The length of loop structures in proteins can range from 2 aa to 22 aa or more, with the shortest being the 2-aa "hairpin loops." The shortest loops figure prominently in the sequentially adjacent structure of Up and Down antiparallel β-barrels (Sibanda and Thornton, 1985). Our previous studies (Mandell et al., 1997a,b,c, 1998) have shown that graphs of $S_{\omega}(\psi_l)$ and discrete and continuous wavelet transformations, $W_{a,b}(\psi_l)$, can help identify and discriminate among secondary structures and their sequential arrangements, such as in β-strands and their loop connectivities.

These studies of the characteristic hydrophobic modes of the hydrophobic free energy eigenfunctions of porins, connexins, GLUTs, potassium channels, and nuclear membrane proteins yield evidence for the β-strand rather than the α-helical structure of their transmembrane segments. In addition, using these methods, we find that these β-strand-dominated proteins can also be discriminated from the characteristic β-strand-containing domains of generic examples of α/β, Greek Key, or Jelly Role β-barrel proteins, which, because of the generally longer and more variable loop connectivities of their β-strands, demonstrate $S_{\omega}(\psi_l)_{l\,=\,1,\,2,\,\text{and/or}\,3}$, with $\omega^{-1} \approx$ 2.2–2.6 aa. In contrast, we find that the porin-like proteins manifest a characteristic higher frequency "β-burst pattern," with wavelengths of $S_{\omega}(\psi_l)_{l\,=\,1,\,2,\,\text{and/or}\,3}$, $\omega^{-1} \approx 2.0$–2.1 aa. Here the β-strand loop connectivities are more strictly 2 aa in length and thus lower the average strand-loop mode length toward the minimum of 2 aa (Sibanda and Thornton, 1985).

We suggest that the "β-burst pattern" is more consistent with the sequentially adjacent, short loop connected β-strands of the Up and Down type, rather than the Greek Key or Jelly Role antiparallel β-barrel types. Comparisons of the graphs of the $W_{a,b}\ (\psi_l)_{l\,=\,1,\,2,\,\text{and/or}\,3}$ of generic examples of these three types of antiparallel β-barrel conformations demonstrate differences in morphology that are consistent with this hypothesis. This conjecture is consistent with the intuition that partial blockade of transmembrane throughput by cross-over connections as in the Greek Key and Jelly Role antiparallel β-barrel conformations would be a less than desirable mechanical arrangement in pore-like β-barrel transmembrane proteins. Tests of this one-dimensional, computationally derived hypothesis await further data from three-dimensional x-ray crystallographic, nuclear magnetic resonance, and other physical studies.

COMPUTATIONAL PROCEDURES

Assignment of hydrophobic free energy values, *H*, to amino acids

There are several amino acid hydrophobicity scales available to transform peptide sequences of transmembrane and other proteins into real numbers (White and Jacobs, 1990; Degli Esposti et al., 1990). From its beginning, our research (Mandell, 1984; Mandell et al., 1987) has utilized the Tanford system of Gibbs-like potential chemical energies in kcal/mol, derived from the relative concentrations of each of the 20 aa at equilibrium in binary aqueous-organic solvents (Nozaki and Tanford, 1971; Manavalen and Ponnuswamy, 1978). This method had its origins in the biophysical chemical research of Edsall and colleagues in the 1930s (Edsall and Wyman, 1958).

H of an amino acid is derived from its "free energy of transfer" from a hydrocarbon solvent to water at 37°C, computed as a chemical potential, μ, from its relative equilibrium concentrations, E_i, in the two media. If E_{HC} and E_W are the equilibrium distributions of an amino acid between the hydrocarbon and water solvents in mole fraction units, and μ_{HC} and μ_W are the corresponding standard chemical potentials, the amino acid's hydrophobic free energy $\equiv H = \mu_W - \mu_{HC} = -RT \ln E_{HC}/E_W$ in kcal/mol (with glycine = 0 as a reference).

The amino acid hydrophobic free energies H in kcal/mol used in these studies are: A = 0.87, R = 0.85, N = 0.09, D = 0.66, C = 1.52, Q = 0.0, E = 0.67, G = 0.0, H = 0.87, I = 3.15, L = 2.17, K = 1.65, M = 1.67, F = 2.87, P = 2.77, S = 0.07, T = 0.07, W = 3.77, Y = 2.76, V = 1.87 (Manavalen and Ponnuswamy, 1978).

It has been shown that H was highly correlated with its aqueous cavity surface area (Reynolds et al., 1974), and we have found that H had a statistically significant correlation ($R^2 = 0.723$, $p = 0.00475$) with a related physical property, the amino acid partial specific volume (in ml/g) (Mandell et al., 1997a; Creighton, 1984).

The amino acid sequences of the proteins that were studied were obtained from the SWISS-PROT Protein Sequence Data Bank. In graphs of the hydrophobic sequences in Figs. 1–4, the H's of proteins of length n were plotted as a function of amino acid sequence position, i.e., $H_{i,\,i\,=\,1\ldots n}$.

Construction of hydropathy plots from $H_{i,\,i\,=\,1\ldots n}$ sequences

Nearest-neighbor, three point moving averages of the $H_{i,\,i\,=\,1\ldots n}$ were iterated 13 times and plotted as a function of the $n - 13$ length for each protein studied. Five-point moving averages iterated 13 times were used to test the stability of the number of sequential maxima in relevant situations.

Construction of hydrophobic free energy eigenfunctions, ψ_l, from $H_{i,\,i\,=\,1\ldots n}$

The $H_{i,\,i\,=\,1\ldots n}$ sequences were used to generate an M-lagged data matrix from which $M \times M$ covariance matrices, C_M, were computed. These C_M were decomposed into sets of l orthogonal eigenfunctions, $\psi_{l(j),\,l\,=\,1\ldots M,\,j\,=\,1\ldots n-M+1}$ (Broomhead and King, 1986; Golub and Van Loan, 1993; Mandell et al., 1997a,b,c, 1998). From the data column

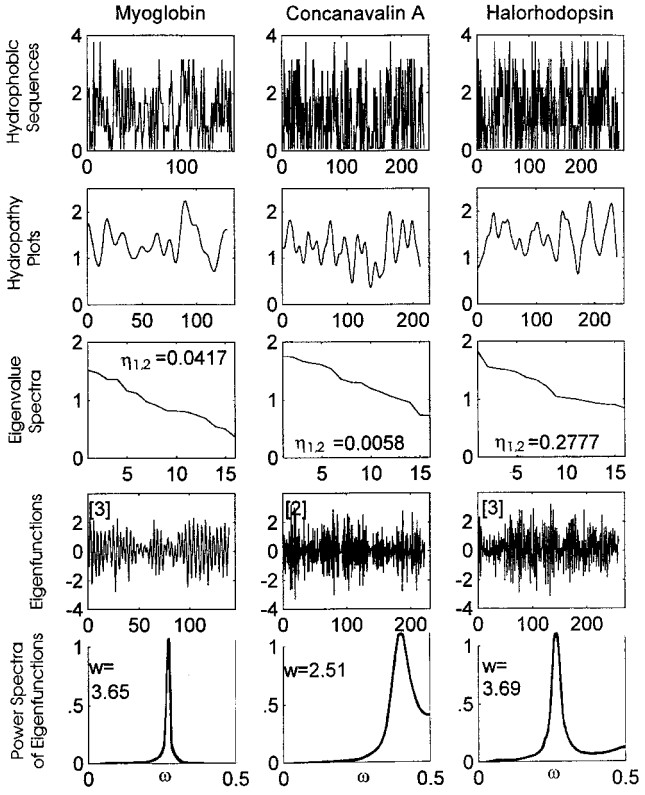

FIGURE 1 Graphs of the linear transformations of the hydrophobic free energy sequences, $H_{i,\ i\ =\ 1\ldots\ n}$, of an α-helical (myoglobin), β-barrel (concanavalan A), and α-helical transmembrane (halorhodopsin) proteins of known physical structure. The first row depicts their amino acid sequences as $H_{i,\ i\ =\ 1\ldots\ n}$ in kcal/mol. The second row contains graphs of their hydropathy plots. The third row contains graphs of the eigenvalue spectra, $\{\nu_i\}_{i\ =\ 1\ldots\ 16}$, of their autocovariance matrices, C_M, computed on their $H_{i,\ i\ =\ 1\ldots\ n}$ sequences and ordered from largest to the smallest. $\eta_{1,2} = \nu_1 - \nu_2/\nu_1 - \nu_M$ is generally >0.2 in proteins with repeating transmembrane segments. The fourth row displays graphs of the hydrophobic free energy eigenfunctions, $\psi_{l,\ l\ =\ 1,\ 2,\ or\ 3}$, that contain the fastest varying hydrophobic free energy frequencies. The bottom row contains graphs of all poles, maximum entropy power spectral transformations of the graphed eigenfunctions, $S_\omega(\psi_l)$, and the ω^{-1} in aa. Note that the hydropathy plot of halorhodopsin demonstrates the seven transmembrane segments characteristic of the general class of G-protein-coupled receptors. The known α-helical dominance of myoglobin is seen in $S_\omega(\psi_3)$, $\omega^{-1} = 3.65$ aa, and the transmembrane segments of halorhodopsin $S_\omega(\psi_3)$, $\omega^{-1} = 3.69$ aa. The hydropathy plot of concanavalin A demonstrates 12 maxima consistent with its 12 β-strands, as is its $S_\omega(\psi_2)$, $\omega^{-1} = 2.51$ aa. See text.

vectors ($T \equiv$ transpose) $V_1^T = (H_1, H_2, \ldots, H_{n-M})$, $V_2^T = (H_2, H_3, \ldots, H_{n-M+1})$, $\ldots$, $V_M^T = (H_M, H_{M+1}, \ldots, H_n)$, and where $K = n - M + 1$, the sequence-averaged dyadic product $H_i H_i^T$ is used to obtain the autocovariance matrix, a Hermitean $M \times M$ matrix, $C_M = 1/K\ \{H_i H_i^T\}$. $M = 16$ was chosen to minimize the least-squares error of many of the protein's ψ_1 from their hydropathy plots. We compute the ordered eigenvalues, $\{\nu_i\}_{i\ =\ 1\ldots\ M}$, and the associated ordered eigenvectors, $X_i(j)$, of C_M, where $i = 1 \ldots M$ and labels the eigenvector, and $j = 1 \ldots M$ and refers to the jth components of the eigenvector X_i. The $\{\nu_i\}_{i\ =\ 1\ldots\ M}$ are ordered from largest to smallest and constitute the eigenvalue spectrum of C_M, which are graphed in Figs. 1–4. The similarly ordered associated $X_i(j)$ are convolved with H_1, H_2, $\ldots$, H_n into $\psi_l(j)$, where $l = 1 \ldots M$ labels the eigenvector and $j = 1 \ldots n - M$ indexes the eigenfunction's jth component.

In words, the convolution of each of the leading eigenvectors with the hydropathy series is carried out by computing the sums of the scalar products of the M length eigenvector with an M length of the hydrophobic series to produce a point in the eigenfunction; this process is translated down the data series by one step and repeated to generate each of the sequential points of the eigenfunction that corresponds to its ordered eigenvalue-associated eigenvector in the computation. In these studies, the $\psi_{l,\ l\ =\ 1,\ 2,\ or\ \ 3\ of\ M}$ are plotted as a function of the M lag-reduced sequence position. We also compute an empirical index on the eigenvalue spectra, $\eta_{1,2} = \nu_1 - \nu_2/\nu_1 - \nu_M$, which tends to be higher in membrane proteins with more hydrophobically prominent transmembrane patterns.

Intuitively, C_M scans for hydrophobic modes across a range of autocorrelation lengths from 1 to M, the range of the lags in the autocovariance matrices. Because C_M is real, symmetrical ($H_{ij} = H_{ij}$) and normal ($C_M C_M^T = C_M^T C_M$), its $\{\nu_i\}_{i\ =\ 1\ldots\ M}$ are real, nonnegative and distinct, and its associated $X_i(j)$ constitute a natural basis for orthonormal projections on $H_1, H_2, \ldots, H_n$ (Golub and Van Loan, 1993). The set of ψ_l can be regarded as orthonormally decomposed sequences of eigenvector-weighted, moving average values (Broomhead and King, 1986).

All-poles, maximum entropy power spectral transformation of the leading eigenfunctions, $S_\omega(\psi_l)$

The ψ_l were transformed into their dominant hydrophobic modes (inverse frequencies, ω^{-1}) by using all-poles, maximum entropy power spectra, $S_\omega(\psi_l)$ (Madan, 1993). Generally, $S(\omega) = a_0/|1 + \Sigma_{k=1\ldots\ M} a_k \exp(ik\omega)|^2$, such that the zeros of the denominator result in peaks ("poles") marking the dominant hydrophobic mode(s) of the ψ_l. This form of the Fourier transformation generates relatively well-resolved spectral peaks in finite series in which only a small number, k, of the (auto)covariance coefficients, c_k, are known. In these studies $k \leq 8$ to avoid "splitting" $S(\omega)$ into spurious modes. The Fourier coefficients, a_k, match the set of k data-derived c_k, chosen so that the entropy of the spectral estimate, $h = \int \ln S(\omega^{-1}) d\omega$, is maximal. Beyond the limited information of the data-derived small set of autocorrelation-matched Fourier coefficients, called the "correlation matching property," the process is extended into a Gaussian process such that h is maximized. It is known that the Gaussian is the function that maximizes h under the constraints of a finite number of second-order c_k as in our data (Madan, 1993). Intuitively, the all-poles, maximum entropy $S(\omega)$ yields results like an autoregressive, maximum likelihood spectral estimate in that it is not mod-

el-dependent, but rather its a_k's follow from the c_k's that are derived directly from the data (Priestly, 1981). This technique acts as a filtering process, yielding the moduli of the one or two leading complex poles of discrete hydrophobic variational frequency in minimally distorted form from the leading ψ_l of protein sequences (Mandell et al., 1997a,b,c, 1998).

Continuous, Mexican hat wavelet transformations, $W_{a,b}(\psi_l)$

$S_\omega(\psi_l)$ locates the dominant modes of the ψ_l of the $H_{i,\ i\ =\ 1\ldots n}$ series in inverse frequency-wavelength space, but positional information is lost. The hypothesis concerning the types of loop connectivities in the β-barrel domains makes it desirable to locate the β-strands and connecting loops represented in the ψ_l in sequence space as well. In contrast to Fourier transformations, wavelet analysis permits the simultaneous assessment of the ψ_i for both wavelength and sequence location in a Heisenberg-like tradeoff of precision between these two dimensions (Wickerhauser, 1994). Wavelet analysis is a more localized and therefore less data length dependent alternative to even windowed Fourier analysis, in which sequence resolution is limited by the arbitrary choice of window size. The one-dimensional wavelet transform can be considered analogous to a local, filtered, Fourier-like transform obtained by dilating and translating the analyzing wavelet, followed by convolving it with the eigenfunction sequence. This amounts to computing all of the correlations between the eigenfunction and the mother wavelet as scaled and translated. The continuous wavelet transform, $W_{a,b}(\psi_l)$, is the sum over the sequence of the $\psi_l(j)$, $_j = 1\ldots n - M + 1$, composed with scaled $(1/a)$ and shifted $(i - b)$ versions of the wavelet function, $w(x)$. "Scaled" as used here is analogous to progressive changes in the inverse radian frequency of a trigonometric function.

In these studies, the "mother wavelet," $w(x)$, is what is called a "Mexican hat," $w(x) = (2 - |x|^2)\exp(-|x|^2/2)$, which is of finite duration, regular, and symmetrical and integrates to 0. The role of a and b is seen in the wavelet transform of $\psi_l(j)$ across j as $W_{a,b}(\psi_l) = a^{-1/2}\int\Psi^l(j)w((j - b)/a)\mathrm{d}j$.

In graphs of these wavelet transformations (Fig. 5), we plot the moduli normalized to 100% for each of the 64 dilate windows (precision optimized for the "Heisenberg-like" tradeoff between location and dilation) and shaded as indicated. Position along the x axis indexes the location along the eigenfunction sequence, and the y axis indicates the relative dilation of the mother wavelet, $w(x)$, which is composed with ψ_l, in 64 dilate divisions (dd). dd can be translated into an approximation of (mother) wavelength in aa. The wavelength of the fastest varying mother wavelet is 2 aa, graphed at the bottom of the wavelet plane. Each dd bin is an increment of $0.5/64 = 0.00781$ in dilation space, such that the inverse frequency (mother wavelength) is $1/0 \rightarrow \infty$ aa at the top of the wavelet graph. With 64 dilate divisions, $\mathrm{dd}_{1\ldots 64}$, the wavelength of a modulus located at dilate division dd is computed as $\omega^{-1} = 1/(0.5 - (\mathrm{dd}(0.5/64)))$ aa.

RESULTS

Fig. 1 contains the graphs of the $H_{i,\ i\ =\ 1\ldots n}$ and ψ_l-related transformations of three physically well-characterized proteins (Fermi and Perutz, 1981; Edelman et al., 1972; Michel, 1982). These examples were chosen to represent proteins with fast frequency-short wavelength hydrophobic variations. Myoglobin, a typical α-helical-dominated globular protein, demonstrates a dominant hydrophobic mode of $S_\omega(\psi_3)$, $\omega^{-1} \approx 3.6$ aa. Concanavalin A, an antiparallel β-strand, Jelly Role barrel domain-containing globular protein, had a dominant mode of $S_\omega(\psi_2)$, $\omega^{-1} \approx 2.5$ aa, and halorhodopsin, a seven α-helical, transmembrane G-protein-coupled membrane protein, yielded a $S_\omega(\psi_3)$, $\omega^{-1} \approx 3.6$ aa.

The top row of Fig. 1 depicts the graphs of the $H_{i,\ i\ =\ 1\ldots n}$ series of these three proteins. The second row contains their hydropathy plots computed as described above. Note that both myoglobin and halorhodopsin manifest about seven hydrophobic maxima, consistent with variously long helical segments of the former and the more regular seven transmembrane segments of the latter (Henderson et al., 1990; Richardson, 1981; Lesk, 1984; Brandon and Tooze, 1991). In comparison with the hydropathy plot of myoglobin, the hydropathy plot of concanavalin A suggests 12 smaller, shorter hydrophobic maxima, approximating the number of β-strands seen in schematic representations of its Jelly Role β-Barrel secondary and supersecondary structure (Richardson, 1981; Lesk, 1984). The third row portrays the eigenvalue spectra, $\{\nu_i\}_{i\ =\ 1\ldots 16}$ of the proteins' $H_{i,\ i\ =\ 1\ldots n}$. A comparison demonstrates the expected more prominent $\eta_{1,2} = 0.2777$ for the transmembrane protein halorhodopsin. We have found that a $\eta_{1,2} > 0.20$ is characteristic of the G-coupled, seven transmembrane receptor proteins that we have studied (Mandell et al., 1997a) and, as will be seen below, most but not all transmembrane pores, channels, and transporters.

The fourth (next to last) row of Fig. 1 is composed of graphs of the eigenfunctions containing the hydrophobic modes relevant to the transmembrane secondary structures, ψ_3, ψ_2, and ψ_3, respectively. ψ_3 was chosen over ψ_2 in the indicated cases (here and in the studies to follow) because their $S_\omega(\psi_2)$'s demonstrated a mixture of the primary and secondary modes of ψ_1 and ψ_3, making $S_\omega(\psi_2)$ bimodal. The bottom row contains the graphs of $S_\omega(\psi_l)_{l\ =\ 2\ \mathrm{or}\ 3}$, demonstrating the dominant hydrophobic modes of the extramembranous and intramembranous α-helices of myoglobin and halorhodopsin, respectively, and extramembranous β-strand-dominated antiparallel Jelly Role β-barrel domains of concanavalan A.

Fig. 2 is a summary of the results of these transformations applied to the $H_{i,\ i\ =\ 1\ldots n}$ of representatives of four different families of plasma membrane-associated proteins. The

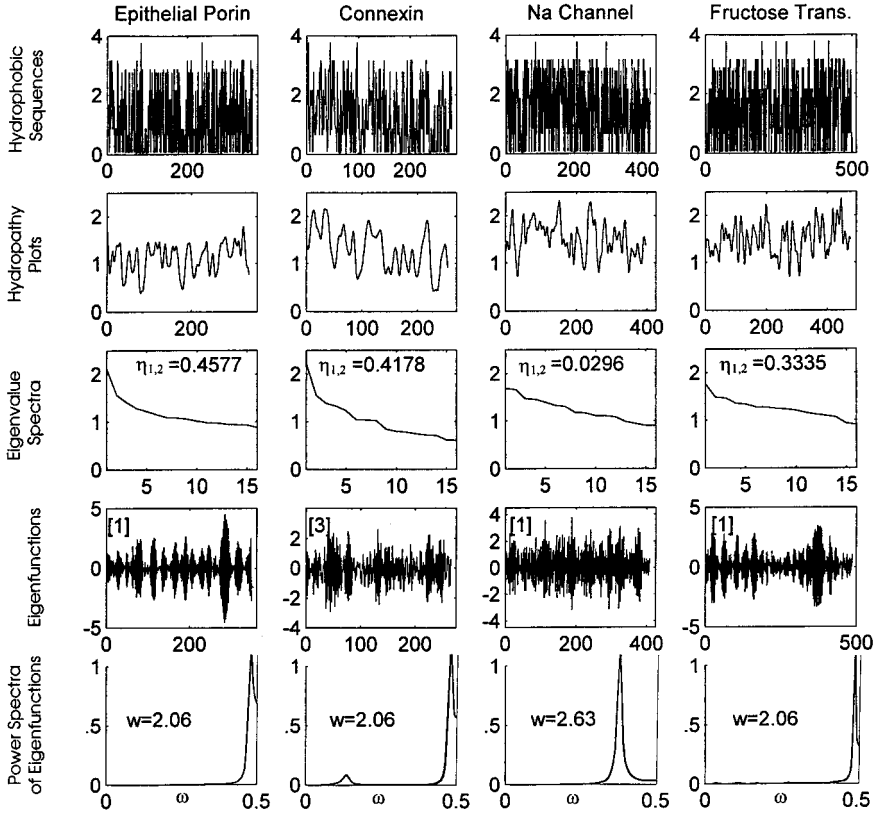

FIGURE 2 The graphs, arranged as in Fig. 1, illustrate the results of transformations of examples of membrane pores (epithelial porin, connexin), an ion channel (brain 1-α subunit of a human sodium channel), and a membrane transporter ($GLUT_5$, the fructose transporter). Notice that the hydropathy plots of porin, the sodium channel, and the fructose transporter demonstrate 16 maxima, whereas that of connexin 32 displays 12. A $\eta_{1,2} \geq 0.20$ is found in the eigenvalue spectra of porin, connexin, and the fructose transporter, but not that of sodium channel subunit. The relevant eigenfunctions of porin, connexin, and fructose transporter, but not of the sodium channel, demonstrate β-burst patterns with their characteristic power spectra, $S_\omega(\psi_1)$, $\omega^{-1} = 2.0$–2.1 aa. The sodium channel exhibits an eigenfunction β-strand wavelength commonly found in a variety of globular proteins and Greek Key and Jelly Role β-barrels, $S_\omega(\psi_1)$, $\omega^{-1} = 2.63$ aa.

OmpF (epithelial) porin of known x-ray structure (Cowan et al., 1992) is an integral membrane protein mediating the passive transport of small hydrophilic molecules across the outer membrane of *E. coli.* Each monomer in this trimeric protein forms a solvent-accessible pore along a barrel axis. Its physical characterizations have confirmed the suggestion of its 16 maxima hydropathy plot (Fig. 2, *second row, leftmost column*) having 16-stranded, sequentially adjacent, membrane-spanning sets of antiparallel β-strands forming a β-barrel (Cowan et al., 1995). The N- and C- termini of the monomers bind via a salt bridge forming a pseudocontinuous strand across the trimer, but in three dimensions the adjacently sequenced antiparallel strands of each monomer are perpendicular to each other. The porin's eigenvalue spectra, $\{\nu_i\}_{i\,=\,1\ldots16}$ (*third row, leftmost column*), have the expected high transmembrane protein value of $\eta_{1,2} = 0.4577$. The porin's ψ_1 (*fourth row, leftmost column*) demonstrates 16 "β-bursts," which we conjecture to be the eigenfunction signature of an antiparallel Up and Down β-barrel transmembrane protein. The S_ω (ψ_1) is in the range of $\omega^{-1} = 2.0$–2.1 aa (*fifth row, leftmost column*). This finding is consistent with our hypothesis that β-burst patterns in eigenfunctions of sequentially adjacent β-strands of Up and Down β-barrels with 2-aa loops are discriminable from those representing β-strands with S_ω (ψ_1), $\omega^{-1} \approx 2.3$–2.6 aa found in globular proteins, including those with antiparallel β-strands with cross-over connections of more variable lengths, such as Greek Key (example: prealbumin, Fig. 4) or Jelly Role (example: concanavalan A, Fig. 1) barrels.

The connexins, a ubiquitous, multigene family of conserved cell surface transmembrane proteins, are the subunits of gap junction channels that directly connect the cytoplasmic compartments of neighboring cells. They have been physically characterized in three dimensions by electron crystallographic methods (Perkins et al., 1997). The transformations of the $H_{i,\,i\,=\,1\ldots n}$ of connexin 32 are portrayed in Fig. 2 (*second column*). From the top to the bottom row, we see the $H_{i,\,i\,=\,1\ldots n}$ sequence, the hydropathy plot with 12 maxima, and its $\{\nu_i\}_{i\,=\,1\ldots16}$ spectrum with a relatively large $\eta_{1,2} = 0.4178$. The fourth row of the second column demonstrates a characteristic β-burst pattern with a $S_\omega(\psi_3)$, $\omega^{-1} \approx 2.0$–2.1 aa (*fifth row, second column*). Although the porins and the connexins belong to different multigene families and differ with respect to their specific amino acid sequences, there exists a "transformational homology" between them, signified by a common β-burst pattern in their relevant hydrophobic free energy eigenfunctions. Again, we conjecture this to be signatory of the short-loop, antiparallel, sequentially adjacent, antiparallel Up and Down β-barrel-containing transmembrane proteins.

Transformations of the $H_{i,\,i\,=\,1\ldots n}$ sequences of porins and connexins contrast with those of the ~400 amino acid, repeating motifs of cloned sodium channel sequences (Stuhmer et al., 1989; Trimmer and Agnew, 1989; Stephan and Agnew, 1991), exemplified by the functionally essential component of the human sodium channel protein, brain 1-α human sodium channel protein subunit (Lu et al., 1992) (Fig. 2, *third column*). Although sharing 16 hydropathy maxima with the potassium channel proteins (Fig. 3) and the

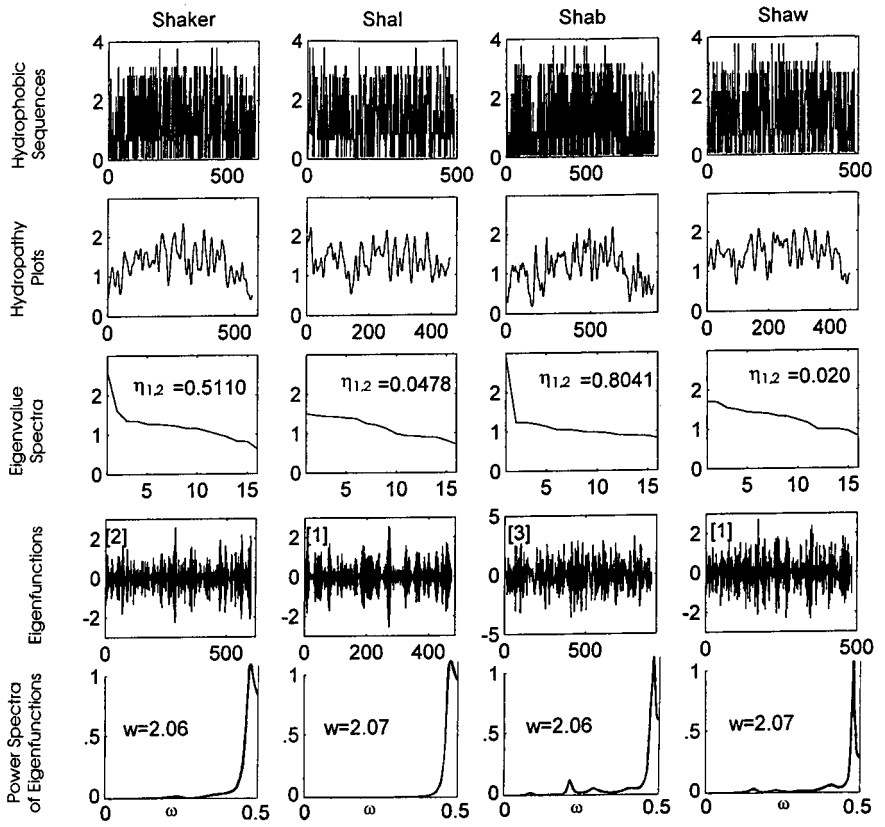

FIGURE 3 Arranged as in Figs. 1 and 2, these graphs demonstrate the results of transformations of the hydrophobicity sequences of the voltage-gated potassium channels belonging to the four indicated gene subfamilies. The 16 small maxima found in these hydropathy plots resemble those of epithelial porin, the sodium channel, and the fructose transporter shown in Fig. 2. $\eta_{1,2} \geq 0.20$ is found in *Shaker* and *Shab* but not in *Shal* and *Shaw* (see text for a discussion of these differences). The porin-like β-burst patterns in the indicated eigenfunctions and their $S_\omega(\psi_1)$, $\omega^{-1} = 2.0$–2.1 aa suggest the presence of Up and Down β-barrel domains in the *Shaker*-related gene families of potassium channels. This pattern contrasts with β-strand eigenfunction wavelength found in the sodium channel subunit of $\omega^{-1} = 2.63$ aa (see Fig. 2).

fructose transporter (Fig. 2, *last column*), the sodium channel protein manifests a relatively low $\eta_{1,2}$. Its ψ_1 is irregular, but not intermittently β-bursting. Consistent with this impression, the sodium channel $S_\omega(\psi_1)$ indicated a β-strand pattern of $\omega^{-1} = 2.63$ aa, the $S_\omega(\psi_2)$ of $\omega^{-1} = 2.63$ aa (not shown), and $S_\omega(\psi_3)$ of $\omega^{-1} = 2.31$ aa (not shown). None of the sodium channel's eigenfunctions demonstrated the $S_\omega(\psi_1)$ of $\omega^{-1} = 2.0$–2.1 aa we are calling a β-burst pattern. This experimentally disconfirmable computational difference between sodium and potassium channels awaits further physical data for evaluation.

The fourth column of Fig. 2 portrays the results of the transformations of the $H_{i,\ i\ =\ 1\ldots\ n}$ of the fructose transporter, $GLUT_5$, one of the superfamily of five isoforms of passive, facilitative hexose transporters with ~65% sequence similarities. These are integral membrane proteins in a variety of organisms and mammalian organs (Silverman, 1991; Elias and Longo, 1992). As noted above, the arbitrary choice of a 21-residue averaging window for hydropathy plots has led to the speculation that the hexose transporters belong to a family of membrane transporter proteins composed of 12 membrane-spanning α-helices (Mueckler et al., 1985; Baldwin, 1990; Kilty and Amara, 1992). The graph resulting from the iterated three-point moving average computation used in these studies (Fig. 2, *fourth column, second row*) suggests that the number of hydrophobic maxima of $GLUT_5$ is ~16, similar to that found in porin and all four of the *Shaker* family of potassium channel proteins portrayed in Fig. 3. The fructose transporter, $GLUT_5$, also demonstrates a relatively large $\eta_{1,2} = 0.3335$. The $GLUT_5$ ψ_1 appears to manifest an intermittent β-burst pattern, which is confirmed by the power spectrum of its leading eigenfunction, $S_\omega(\psi_1)$ of $\omega^{-1} = 2.06$ aa. These findings are consistent with the speculation that the hexose transporters may be 16-stranded, β-barrel proteins (Fischbarg et al., 1994). These results also suggest that the dominant domains of the fructose transporter are sequentially adjacent, antiparallel Up and Down β-barrels.

Fig. 3 summarizes the results of our studies of the voltage-gated potassium channels belonging to four gene subfamilies: *Shaker, Shal, Shab*, and *Shaw*, common to metazoans ranging from mollusks and arthropods through vertebrates (Wei et al., 1990; Jan and Jan, 1990; McCormack et al., 1990; Jegla et al., 1995; Yao et al., 1996). The *Shaker* family of potassium channels can vary greatly in amino acid composition in that its genes have a large number of exons that produce a wide variety of splice variants, even in regions of the ion selective pores (Kim et al., 1997). A common model for this A-type to inward rectifying range of potassium channels contains four homologous (but possibly heterotetrameric) subunits, each of which is said to have two hydrophobic segments called M1 and M2. It has been speculated by some that M1 and M2 are α-helices. Using glycosylation in studies of ROMK1, the generic potassium channel, additional transmembrane segments have been suggested (Schwalbe et al., 1997). The potassium channel pore regions have also been modeled, with varying success, using both a tetramer of membrane-

spanning β-hairpins (e.g., an eight-stranded antiparallel Up and Down β-barrel) and a tetramer of incompletely membrane-spanning α-helical hairpins (e.g., an eight-component α-helical bundle) (Kerr and Sansom, 1997). In a study using scanning mutagenesis, the systematic sequential substitution with hydrophobic and charged amino acids in these segments failed to demonstrate α-helical periodicity in their functional tolerance to substitution (Collins et al., 1997), whereas another study using point substitutions of two amino acids of widely different hydrophobicities produced results consistent with M2 being an 18-residue straight α-helix (Choe et al., 1995). On the other hand, dichroic ratios of two amide bands with parallel and perpendicular polarizations in β-sheet structures have been shown to be relevant to both potassium channel-associated peptides and the porins (Marsh, 1997). Other speculation about the *Shaker*, *Shal*, *Shab*, and *Shaw* gene families is that there are six transmembrane segments (S_1–S_6), with S_4, due to its density of charged amino acids, suggested to be the voltage-sensor component.

Graphs of the $H_{i,\ i\ =\ 1\ldots\ n}$ constitute the first row of Fig. 3. The hydropathy plots in the second row demonstrate 16 local maxima with a morphology generally similar to that of epithelial porin and the fructose transporter shown in Fig. 2. Sixfold iteration of the 13-fold nearest-neighbor averaging algorithm (not shown) left 16 peaks still countable. The eigenvalue spectra, $\{\nu_i\}_{i\ =\ 1\ldots\ 16}$, of *Shaker* and *Shab* (Fig. 3, *third row*) are associated with large $\eta_{1,2}$, 0.5110 and 0.8041, respectively, whereas *Shal* and *Shab* are not. The source of these differences is not clear from our computations, although we note that the α-subunit of the human sodium channel protein (Fig. 2) is also without the $\eta_{1,2} >$ 0.20 of most of the transmembrane proteins that we have studied. Because eigenvalues of autocovariance matrices are more prominent when the underlying function is more regularly varying, the relatively low values of $\eta_{1,2}$ in these transmembrane proteins may reflect more irregularity in their hydrophobic transmembrane loops. Our finding of β-bursting in ψ_1 (not ψ_2 or ψ_3) of the two potassium channel proteins with low values of $\eta_{1,2}$ is consistent with this descriptive explanation. Thus the fourth and fifth rows of Fig. 3 suggest the presence of β-burst containing ψ_i with S_ω (ψ_{1-3}) = 2.0–2.1 aa. This finding, in addition to the porin-like 16 local maxima in the hydropathy plots, suggests the presence of Up and Down β-barrel domains in the *Shaker* gene-related families of potassium channels. In an examination of a more generic potassium channel protein, we found that the ψ_2 of ROMK1 demonstrates a porin-like β-burst pattern with a $S_\omega(\psi_2)$ of ω^{-1} = 2.04 aa. $S_\omega(\psi_1)$ of ROMK1 yielded ω^{-1} = 4.31 aa.

We examined the possibility that leading hydrophobic free energy eigenfunctions with β-burst patterns might also be found in pore-like proteins associated with subcellular membranes. The first two columns of Fig. 4 portray the transformations of the $H_{i,\ i\ =\ 1\ldots\ n}$ of two proteins associated with the nuclear membrane. NU98 (98 kDa in molecular mass) is a member of the nucleoporin family, a component

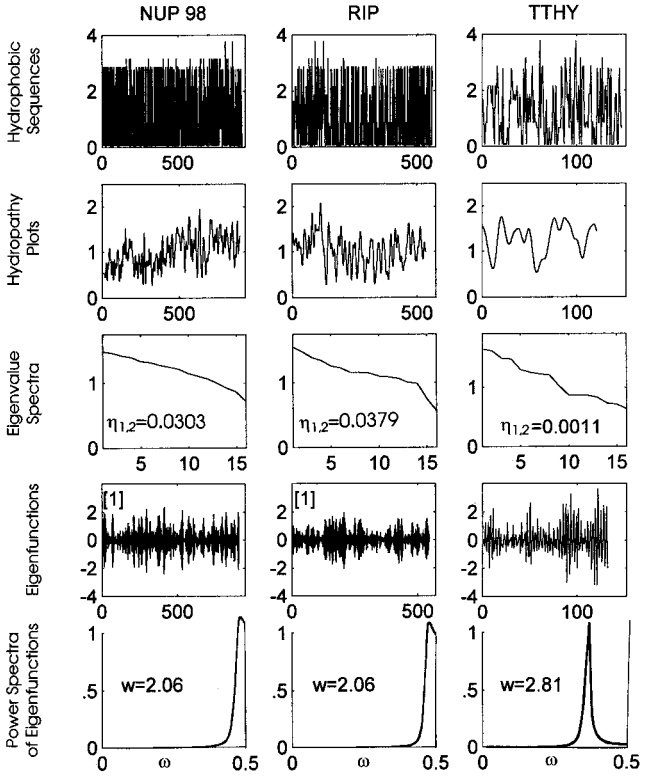

FIGURE 4 Arranged as in the previous figures, these graphs represent the results of the transformations of the hydrophobic free energy sequences of two nuclear membrane-associated proteins, NUP98 and RIP, and a plasma thyroid hormone binding protein, TTHY. TTHY is exhibited here as a generic example of a protein containing a Greek Key antiparallel β-barrel domain, for contrast with concanavalin A (Jelly Role) in Fig. 1 and porin (Up and Down) in Fig. 2. Both NUP98 and RIP are components of nuclear pore complexes involved with the transport of metabolic material between nucleus and cytoplasm. The hydropathy plots indicate ~16 small maxima in RIP and 30–32 in NUP98, which is almost twice as long. The ψ_1 of both demonstrate a β-burst pattern and associated $S_\omega(\psi_1)$, ω^{-1} = 2.0–2.1 aa, suggestive of the Up and Down antiparallel β-barrel pattern. The approximately eight maxima found in the hydropathy plot of TTHY are consistent with x-ray data suggesting that the protein contains two four-stranded β-sheets, and TTHYs $S_\omega(\psi_1)$, ω^{-1} = 2.81 aa, a relatively high average β-strand wavelength, is consistent with x-ray evidence for both the β-strands and loop connectivities having variable lengths. See text for more details.

of nuclear pore complexes involved with the transport of nucleic acids, proteins, and metabolites between the cell nucleus and cytoplasm (Kubitscheck et al., 1996; Belgareh and Doye, 1997). RIP (Rev interacting protein) is also a nuclear pore complex component thought to interact with HIV-1 Rev protein and to play a role in RNA export (Zapp, 1995). The hydropathy plot of RIP (Fig. 4, *second row*) demonstrates 16 small peaks, not unlike the families of potassium channels in Fig. 3 and the fructose transporter in Fig. 2. The hydropathy plot of NUP98, with almost twice the molecular mass of RIP, has 30–32 small peaks. The eigenvalue spectra of both resemble those of *Shal* and *Shab* (Fig. 3) with $\eta_{1,2} < 0.20$. The β-burst pattern is observed in the ψ_1 of both nuclear membrane proteins (Fig. 4, *fourth row*), as are both their associated $S_\omega(\psi_1)$ of ω^{-1} = 2.06 aa.

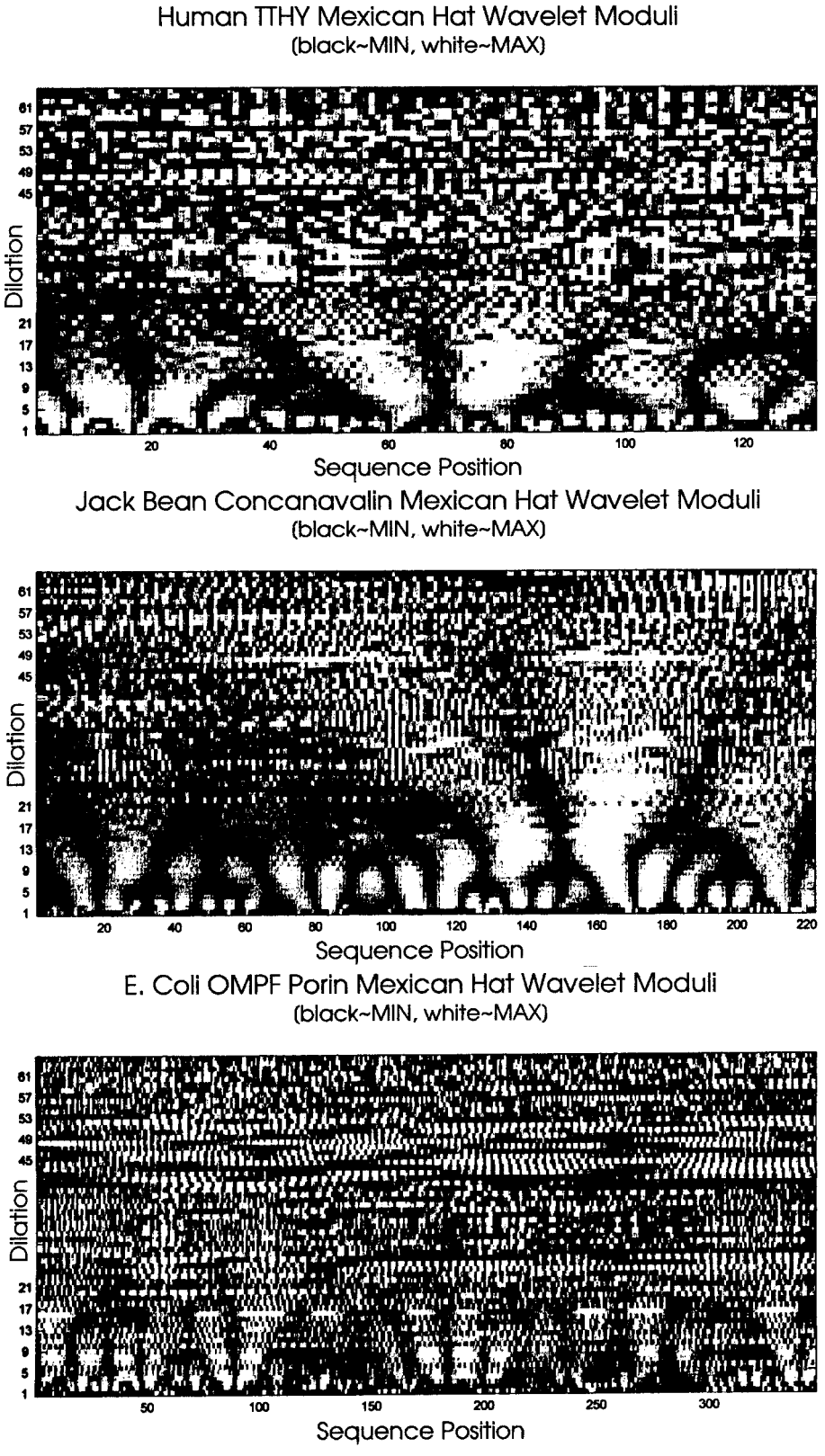

FIGURE 5 Graphs of the moduli of continuous wavelet transformations of the β-strand containing eigenfunctions, $W_{a,b}(\psi_1)$, and of examples of three types of antiparallel β-structure-containing proteins: Greek Key (the ψ_1 of TTHY), Jelly Role (the ψ_2 of concanavalin A), and Up and Down (the ψ_1 of OMPF porin) as a function of position (x axis) and dilate wavelength (y axis). Each of the 64 dilate ranges was normalized to 100%, and the modular amplitudes grey scale were coded from black (relative minimum) to white (relative maximum). The y axis ranges in wavelength from $\omega^{-1} = 1/.5 = 2$ aa to $\omega^{-1} = 1/0 = \infty$ aa in 64 dilate bands. The dilate-to-amino acid wavelength transformation was computed as indicated in the text. Although there is some ambiguity with respect to the number of β-moduli in the hydropathy plots, there appear to be eight in TTHY with $W_{a,b}(\psi_1)$, $\omega^{-1} = 2.21$–2.92 aa, 12–16 in concanavalin A with $W_{a,b}(\psi_2)$, $\omega^{-1} = 2.21$–2.92 aa. and 16 in the porin with $W_{a,b}(\psi_1)$, $\omega^{-1} = 2.04$–2.27 aa. As suggested by the $S_\omega(\psi_1)$ of these proteins (Figs. 1, 2, and 4), the maximum moduli in the β-strand regions have longer and less uniform wavelengths in Greek Key TTHY and Jelly Role concanavalin A than in the Up and Down type porin, in which they are shorter and more uniform. See text.

This extends the antiparallel Up and Down β-barrel domain computational hypothesis beyond the porins, connexins, potassium channels, and the GLUT transporters to nuclear membrane proteins.

For comparison with the antiparallel, Up and Down, and Jelly Role β-barrel (concanavalan A, Fig. 1) domain-containing proteins as described above, the third column of Fig. 4 contains the results of transformations of a generic Greek

Key, antiparallel β-barrel protein, transthyretin (TTHY), previously called prealbumin (Richardson, 1981). X-ray studies have characterized the supersecondary structure of TTHY as a "sandwich" of two four-stranded β-sheets, with both their β-strands and loop connections having variable lengths. The hydropathy plot of TTHY displays eight maxima, suggestive of the sequence locations and relative lengths of its eight β-strands. As expected, the eigenvalue spectra and $\eta_{1,2}$ of this plasma protein are without indications of transmembrane structure. TTHY's ψ_1 (*fourth row*) demonstrates irregularly bunched β-strand-like hydrophobic free energy oscillations with $S_\omega(\psi_1)$ of $\omega^{-1} = 2.81$ aa. The $S_\omega(\psi_2)$ of $\omega^{-1} = 7.69$ aa (not shown) suggests the averaged length of its eight β-strands. $S_\omega(\psi_3)$ was bimodal, containing both the peaks of $S_\omega(\psi_1)$ and $S_\omega(\psi_2)$. We conclude that the proteins that served as examples of Jelly Role (concanavalin A, $S_\omega(\psi_2)$ of $\omega^{-1} = 2.51$ aa) and Greek Key (TTHY, $S_\omega(\psi_2)$ of $\omega^{-1} = 2.81$ aa) antiparallel β-structures were discriminable from those with the β-burst signatory $S_\omega(\psi_i)$ of $\omega^{-1} = 2.0$–2.1 aa of the Up and Down antiparallel β-barrel proteins.

We also compared these three types of antiparallel β-strand-containing proteins, using the length-insensitive wavelet transformation of their β-strand-containing eigenfunctions. $W_{a,b}(\psi_1)$ is particularly suited for the assessment of local frequency content. Fig. 5 depicts the graphs of the $W_{a,b}(\psi_1)$ of TTHY, the $W_{a,b}(\psi_2)$ of concanavalin A, and the $W_{a,b}(\psi_1)$ of OMPF porin, using a Mexican Hat mother wavelet. We note that the modular amplitudes are grey-scale-coded from black (relative minimum) to white (relative maximum) by dilate scale, not across all dilate scales. That is, the relative absolute amplitudes in each of the dilate ranges were normalized to 100%. These ψ_i were chosen for wavelet analysis because they most clearly portrayed the β-strands.

In the wavelet graph (Fig. 5) of the ψ_1 of the antiparallel Greek Key β-barrel protein TTHY, we see eight sequential modular maxima, suggestive of the eight known β-strand-loop structures. Two dilate regions are apparent, an observation suggestive of the shorter and longer loop connectivities described in Greek Key β-barrel domains (Richardson and Richardson, 1990). The dilate range of this sequence of secondary structures can be approximated as $\omega^{-1} = 2.21$–2.92 aa (see above for wavelet dilate to wavelength transformation). The graph of the $W_{a,b}(\psi_2)$ of concanavalin A exemplifies a Jelly Role antiparallel β-barrel protein with ~12–16 β-strand-loop moduli with dilate wavelengths of greater variability, $\omega^{-1} = 2.14$–4.31 aa. Both of these modular patterns have longer and more variable wavelengths than that of OMPF porin's 16 modular peaks at $\omega^{-1} = 2.04$–2.27 aa, an exemplar of antiparallel Up and Down β-barrel proteins. It appears that the $S_\omega(\psi_1)$ and $W_{a,b}(\psi_1)$ transformations are in general agreement with respect to the relative wavelengths of the wavelet moduli of these examples of the three types of antiparallel β-barrel proteins.

This work was supported by a National Institute of Mental Health, Small Business Innovation Research grant R43 MH58026-01 to the Cielo Institute (Asheville, NC).

REFERENCES

Baldwin, S. A. 1990. Molecular mechanisms of sugar transport across mammalian and microbial cell membranes. *Biochem. Soc. Trans.* 20: 533–537.

Belgareh, N., and V. Doye. 1997. Dynamics of nuclear pore distribution in nucleoporin mutant yeast cells. *J. Cell. Biol.* 136:747–759.

Branden, C., and J. Tooze. 1991. Introduction to Protein Structure. Garland, New York.

Broomhead, D. S., and G. P. King. 1986. Extracting qualitative dynamics from experimental data. *Physica D.* 20:217–236.

Choe, S., C. F. Stevens, and J. M. Sullivan. 1995. Three distinct structural environments of a transmembrane domain in the inwardly rectifying potassium channel ROMK1 defined by perturbation. *Proc. Natl. Acad. Sci. USA.* 92:12046–12049.

Collins, A., H. Chuang, Y. N. Jan, and L. Y. Jan. 1997. Scanning mutagenesis of the putative transmembrane segments of Kir2.1, an inward rectifier potassium channel. *Proc. Natl. Acad. Sci. USA.* 94:5456–5460.

Cowan, S. W., R. M. Garavito, J. N. Jansonius, J. A. Jenkins, and R. A. Pauptit. 1995. *Structure.* 3:1041–1050.

Cowan, S. W., T. Schirmer, G. Rummel, M. Steiert, R. Ghosh, R. A. Pauptit, J. N. Jansonius, and J. P. Rosenbusch. 1992. Crystal structures explain functional properties of two *E. coli* porins. *Nature.* 358:727–733.

Creighton, T. E. 1984. Proteins; Structures and Molecular Principles. Freeman. New York. 7.

Degli Esposti, M., M. Crimi, and G. Venturoli. 1990. A critical evaluation of the hydropathy profile of membrane proteins. *Eur. J. Biochem.* 190:207–219.

Edelman, G. M., B. A. Cunningham, G. N. Reeke, and J. W. Becker. 1972. The covalent and three-dimensional structure of concanavalin A. *Proc. Natl. Acad. Sci. USA.* 69:2580–2584.

Edsall, J. T., and J. Wyman. 1958. Biophysical Chemistry. Academic Press, New York.

Eisenberg, D., and W. Kauzmann. 1968. The Structure and Properties of Water. Oxford University Press, Oxford.

Eisenberg, D., R. M. Weis, and T. C. Terwilliger. 1984. The hydrophobic moment detects periodicity in protein hydrophobicity. *Proc. Natl. Acad. Sci. USA.* 82:140–144.

Elias, L. J., and N. Longo. 1992. Glucose transporters. *Annu. Rev. Med.* 43:377–393.

Engelman, D. M., T. A. Steitz, A. Goldman. 1986. Identifying nonpolar transbilayer helices in amino acid sequences of membrane proteins. *Annu. Rev. Biophys. Biophys. Chem.* 15:321–353.

Fasman, G. D., and W. A. Gilbert. 1990. The prediction of transmembrane protein sequences and their conformation: an evaluation. *Trends Biochem. Sci.* 15:89–95.

Fermi, G., and M. F. Perutz. 1981. Atlas of Molecular Structures in Biology. Vol. 2. Haemoglobin and Myoglobin. Clarendon, Oxford.

Fischbarg, J., M. Cheung, J. Li, and P. Iserovich. 1994. Are most transporters and channels beta barrels? *Mol. Cell. Biochem.* 140:147–162.

Golub, G. H., and C. F. Van Loan. 1993. Matrix Computations. Johns Hopkins University Press, Baltimore.

Gu, H., J. Ahn, M. J. Caplan, R. D. Blakely, and G. Rudnick. 1996. Cell-specific sorting of biogenic amine transporters expressed in epithelial cells. *J. Biol. Chem.* 271:18100–18106.

Gu, H., S. C. Wall, and G. Rudnick. 1994. Stable expression of biogenic amine transporters reveals differences in inhibitor sensitivity, kinetics and ion dependence. *J. Biol. Chem.* 269:7124–7130.

Henderson, R., J. M. Baldwin, T. A. Ceska, F. Zemlin, E. Beckmann, and K. H. Downing. 1990. Model for the structure of bacteriorhodopsin based on high-resolution electron cryo-microscopy. *J. Mol. Biol.* 213: 899–929.

Jan, L. Y., and Y. N. Jan. 1990. How might the diversity of potassium channels be generated? *Trends Neurosci.* 13:415–419.

Jegla, T., N. Grigoriev, W. J. Gallin, L. Salkoff, and A. N. Spencer. 1995. Multiple Shaker potassium channels in a primitive metazoan. *J. Neurosci.* 15:7989–7999.

Kerr, I. D., and M. S. Sansom. 1997. The pore-lining region of Shaker voltage-gated potassium channels: comparison of β-barrel and α-helix bundle models. *Biophys. J.* 73:581–602.

Kilty, J. E., and S. G. Amara. 1992. Families of twelve transmembrane domain transporters. *Curr. Opin. Biotechnol.* 3:675–682.

Kim, M., D. J. Baro, C. C. Lanning, and M. Doshi. 1997. Alternative splicing in the pore-forming region of Shaker potassium channels. *J. Neurosci.* 17:8213–8224.

Kimura, Y., D. G. Vassylyev, A. Miyazawa, A. Kidera, M. Matsushima, K. Mitsuoka, K. Murata, T. Hirai, and Y. Fujiyoshi. 1997. Surface of bacteriorhodopsin revealed by high resolution electron crystallography. *Nature.* 389:206–211.

Kubitscheck, U., P. Wedekind, O. Zeidler, M. Grote, and R. Peters. 1996. Single pores visualized by confocal microscopy and image processing. *Biophys. J.* 70:2067–2077.

Kyte, J., and R. F. Doolittle. 1982. A simple method for displaying the hydropathic character of a protein. *J. Mol. Biol.* 157:105–132.

Lesk, A. M. 1984. Themes and contrasts in protein structures. *Trends Biochem. Sci.* 9:000–000.

Levitt, M., and C. Chothia. 1976. Structural patterns in globular proteins. *Nature.* 261:552–558.

Lu, C. M., J. Han, T. A. Rado, and G. B. Brown. 1992. Differential expression of two sodium channel subtypes in human brain. *FEBS Lett.* 303:53–58.

Madan, R. N. 1993. All poles, maximum entropy power spectra. *In* Maximum Entropy and Bayesian Methods. A. Mohammad-Djafaro amd G. Demoments, editors. Kluwer, Dordrecht, The Netherlands. 49–54.

Manavalen, P., and P. K. Ponnuswamy. 1978. Hydrophobic character of amino acid residues in globular proteins. *Nature.* 275:673–674.

Mandell, A. J. 1984. Non-equilibrium behavior of some brain enzyme and receptor systems. *Annu. Rev. Pharmacol. Toxicol.* 24:237–274.

Mandell, A. J., P. V. Russo, and B. W. Blomgren. 1987. Geometric universality in brain allosteric protein dynamics: complex hydrophobic transformation predicts mutual recognition by polypeptides and proteins. *Ann. N.Y. Acad. Sci.* 504:88–117.

Mandell, A. J., K. A. Selz, and M. F. Shlesinger. 1997a. Mode matches and their locations in the hydrophobic free energy sequences of peptide ligands and their receptor eigenfunctions. *Proc. Natl. Acad. Sci. USA.* 94:13576–13581.

Mandell, A. J., K. A. Selz, and M. F. Shlesinger. 1997b. Wavelet transformation of protein hydrophobicity sequences suggests their memberships in structural families. *Physica A.* 244:254–262.

Mandell, A. J., K. A. Selz, and M. F. Shlesinger. 1997c. Hydrophobic free energy eigenfunctions help define continuous wavelet transformations of amino acid sequences of protein families. *In* Proceedings of the International School of Physics, Enrico Fermi Course, CXXXIV. F. Mallamace and H. E. Stanley, editors. I. O. S. Press, Amsterdam. 175–192.

Mandell, A. J., K. A. Selz, and M. F. Shlesinger. 1998. Mode matches in hydrophobic free energy eigenfunctions predict peptide-protein interactions. *Biopolymers.* 46:89–101.

Marsh, D. 1997. Dichroic ratios in polarized Fourier transform infrared for nonaxial symmetry of β-sheet structures. *Biophys. J.* 72:2710–2718.

McCormack, T., E. C. Vega-Saenz de Miera, and B. Rudy. 1990. Molecular cloning of a member of a third class of Shaker-family K^+ channel genes in mammals. *Proc. Natl. Acad. Sci. USA.* 87:5227–5231.

Michel, H. 1982. Three-dimensional crystals of a membrane protein complex. *J. Mol. Biol.* 158:567–572.

Mueckler, M., C. Caruso, S. A. Baldwin, M. Panico, I. Blench, H. R. Morris, W. J. Allard, G. E. Lienhard, and H. F. Lodish. 1985. Sequence and structure of a human glucose transporter. *Science.* 229:941–945.

Nozaki, Y., and C. Tanford. 1971. The solubility of amino acids and two glycine peptides in aqueous ethanol and dioxane solutions. *J. Biol. Chem.* 246:2211–2217.

Pauptit, R. A., T. Schirmer, J. N. Jansonius, and J. P. Rosenbusch. 1991a. A common channel-forming motif in evolutionarily distant porins. *J. Struct. Biol.* 107:136–145.

Pauptit, R. A., H. Zhang, G. Rummel, and T. Schirmer. 1991b. Trigonal crystals of porin from Escherichia coli. *J. Mol. Biol.* 218:505–507.

Perkins, G., D. Goodenough, and G. Sosinsky. 1997. Three-dimensional structure of the gap junction connexon. *Biophys. J.* 72:533–544.

Priestly, M. D. 1981. Spectral Analysis and Time Series. Academic Press. San Diego. 600.

Rees, D. C., L. DeAntonio, and D. Eigenberg. 1989. Hydrophobic organizaion of membrane proteins. *Science.* 245:510–513.

Reynolds, J. A., D. B. Gilbert, and C. Tanford. 1974. Empirical correlation between hydrophobic free energy and aqueous cavity surface area. *Proc. Natl. Acad. Sci. USA.* 71:2925–2927.

Richardson, J. S. 1975. Handedness of crossover connections in β-sheets. *Proc. Natl. Acad. Sci. USA.* 72:1349–1353.

Richardson, J. S. 1977. β-sheet topology and the relatedness of proteins. *Nature.* 268:495–500.

Richardson, J. S. 1981. The anatomy and taxonomy of protein structures. *Adv. Protein Chem.* 34:168–339.

Richardson, J. S., and D. C. Richardson. 1990. The origami of proteins. *In* L. M. Gierasch and J. King, editors. AAAS, Washington, DC.

Rose, G. D. 1978. Prediction of chain turns in globular proteins on a hydrophobic basis. *Nature.* 272:586–590.

Schwalbe, R. A., L. Bianchi, and A. M. Brown. 1997. Mapping the kidney potassium channel, ROMK1. Glycosylation of the pore signature sequence and the COOH terminus. *J. Biol. Chem.* 272:25217–25223.

Sibanda, B. L., and J. M. Thornton. 1985. β-hairpin families in globular proteins. *Nature.* 316:170–174.

Silverman, M. 1991. Structure and function of hexose transporters. *Annu. Rev. Biochem.* 60:757–794.

Sonders, M. S., and S. G. Amara. 1996. Channels in transporters. *Curr. Opin. Neurobiol.* 6:294–302.

Stephan, M., and W. S. Agnew. 1991. Voltage-sensitive channels: motifs, modes and modulation. *Curr. Opin. Cell. Biol.* 3:676–684.

Stuhmer, W., F. Conti, H. Suzuki, X. D. Wang, and S. Numa. 1989. Structural parts involved in activation and inactivation of the sodium channel. *Nature.* 339:597–603.

Trimmer, J. A., and Agnew, W. S. 1989. Molecular diversity of voltage-sensitive Na^+ channels. *Annu. Rev. Physiol.* 51:401–418.

Unger, V. M., P. A. Hargave, J. M. Baldwin, and G. F. X. Schertler. 1997. Arrangement of rhodopsin transmembrane α-helices. *Nature.* 389: 203–206.

Wei, A., M. Covarrubias, A. Butler, K. Baker, M. Pak, and L. Salkoff. 1990. K^+ current diversity is produced by an extended gene family conserved in *Drosophilia* and mouse. *Science.* 248:599–603.

White, S. H., and R. E. Jacobs. 1990. Statistical distribution of hydrophobic residues along the length of protein chains. *Biophys. J.* 57:911–921.

Wickerhauser, M. V. 1994. Adapted Wavelet Analysis from Theory to Software. Peters, Wellesley, MA. 103–154.

Wilmot, C. M., and J. M. Thornton. 1988. Analysis and prediction of the different types of β-turns in proteins. *J. Mol. Biol.* 203:221–232.

Yao, X., A. Y. Chang, E. L. Boulpaep, A. S. Segal, and G. V. Desir. 1996. Molecular cloning of a glibenclamide-sensitive, voltage-gated potassium channel expressed in rabbit kidney. *J. Clin. Invest.* 97:2525–2533.

Zapp, M. 1995. The ins and outs of RNA nucleocytoplasmic transport. *Curr. Opin. Genet. Dev.* 5:229–233.